Novel silica/poly(2,6-dimethyl-1,4-phenylene oxide) hybrid anion-exchange membranes for alkaline fuel cells: Effect of silica content and the single cell performance

Yonghui Wu[a], Cuiming Wu[b], John R. Varcoe[c], Simon D. Poynton[c], Tongwen Xu[a,*], Yanxun Fu[a]

[a] CAS Key Laboratory of Soft Matter Chemistry, Laboratory of Functional Membranes, School of Chemistry and Materials Science,
University of Science and Technology of China, Hefei, Anhui 230026, PR China
[b] School of Chemical Engineering, Hefei University of Technology, Hefei, Anhui 230009, PR China
[c] Chemical Sciences, The University of Surrey, Guildford, Surrey GU2 7XH, United Kingdom

A R T I C L E   I N F O

A B S T R A C T

Poly(2,6-dimethyl-1,4-phenylene oxide) (PPO)-based organic–inorganic hybrid alkaline membranes with enhanced hydroxyl (OH^-) conductivity are prepared in response to the relatively low conductivity of previously reported PPO-based systems. The membranes also exhibit higher swelling-resistant properties and the hydroxyl (OH^-) conductivity values are comparable to previously reported fluoropolymer-containing membranes: 0.012–$0.035\,S\,cm^{-1}$ in the temperature range 30–90 °C. Other favorable properties for fuel cell application include high tensile strengths up to 25 MPa and large ion-exchange capacities in the range 2.01–$2.27\,mmol\,g^{-1}$. Beginning-of-life fuel cell testing of a membrane with a thickness of 140 µm yielded an acceptable H_2/O_2 peak power density of $32\,mW\,cm^{-2}$ when incorporated into an alkaline membrane electrode assembly. Therefore, this class of hybrid membrane is suitable for application in alkaline membrane fuel cells.

1. Introduction

Compared with proton exchange membrane fuel cells (PEM-FCs), the advantages of alkaline membrane fuel cells (AMFCs) [1] lie in reduced methanol crossover, enhanced catalyst efficiency and electrokinetics, a higher diversity of catalysts [2], and easy water management [3–6].

Membranes are often a key factor in determining the efficiency and lifetime of fuel cells. One of the challenges in the current AMFC research is to develop hydroxyl (OH^-) conductive membranes with high mechanical properties, low swelling, resistance to alkali-related degradation [7], high conductivity, and acceptable thermal stability [1,8]. High performance AMFCs have been tested with alkaline membranes based on radiation-grafted partially fluorinated poly(ethylene-co-tetrafluoroethylene) (ETFE) films [3,5] and fully fluorinated poly(hexafluoropropylene-co-tetrafluoroethylene) films [9], which have high conductivities (up to $>0.06\,S\,cm^{-1}$ at 60 °C [10]). However, some of their

properties need further optimization, such as the unsuitable mechanical properties [5,9]. Another drawback is the high cost.

Meanwhile, non-fluorinated polymer electrolytes have been developed for application in AMFCs, based on polyvinyl alcohol (PVA) [11], polyethersulfones [12], poly(phthalazinon ether sulfone ketone) [13], polysulfone [14] and poly(2,6-dimethyl-1,4-phenylene oxide) (PPO) [15–17]. To overcome the inherent disadvantages of these polymers (mechanical, thermal, and chemical stabilities) the polymers have been modified by physical blending [15], chemical functionalization [12], and/or cross-linking [11]. A more recently developed modification method is incorporation of inorganic components into polymers to form organic–inorganic hybrid membranes [18]. Although it has not been widely applied, the latter method has the potential for improvement on membrane properties. For instance, we recently prepared a series of anion-exchange hybrid membranes, by incorporation of a fixed content of silica into PPO with thermal treatments at different temperatures, which exhibited superior tensile properties and favorable thermal stabilities [16]. The alkaline resistance is comparable to those of membranes based on partially fluorinated-polymers [19]. Unfortunately, the hydroxyl (OH^-) conductivities, in the range of 0.001–$0.0085\,S\,cm^{-1}$, were too low and the swelling of these membranes needed to be reduced.

* Corresponding author at: Department of Chemistry, University of Science and Technology of China, Jinzai Road 96#, Hefei, Anhui 230026, PR China.
Tel.: +86 551 360 1587; fax: +86 551 3601592.
E-mail address: twxu@ustc.edu.cn (T. Xu).
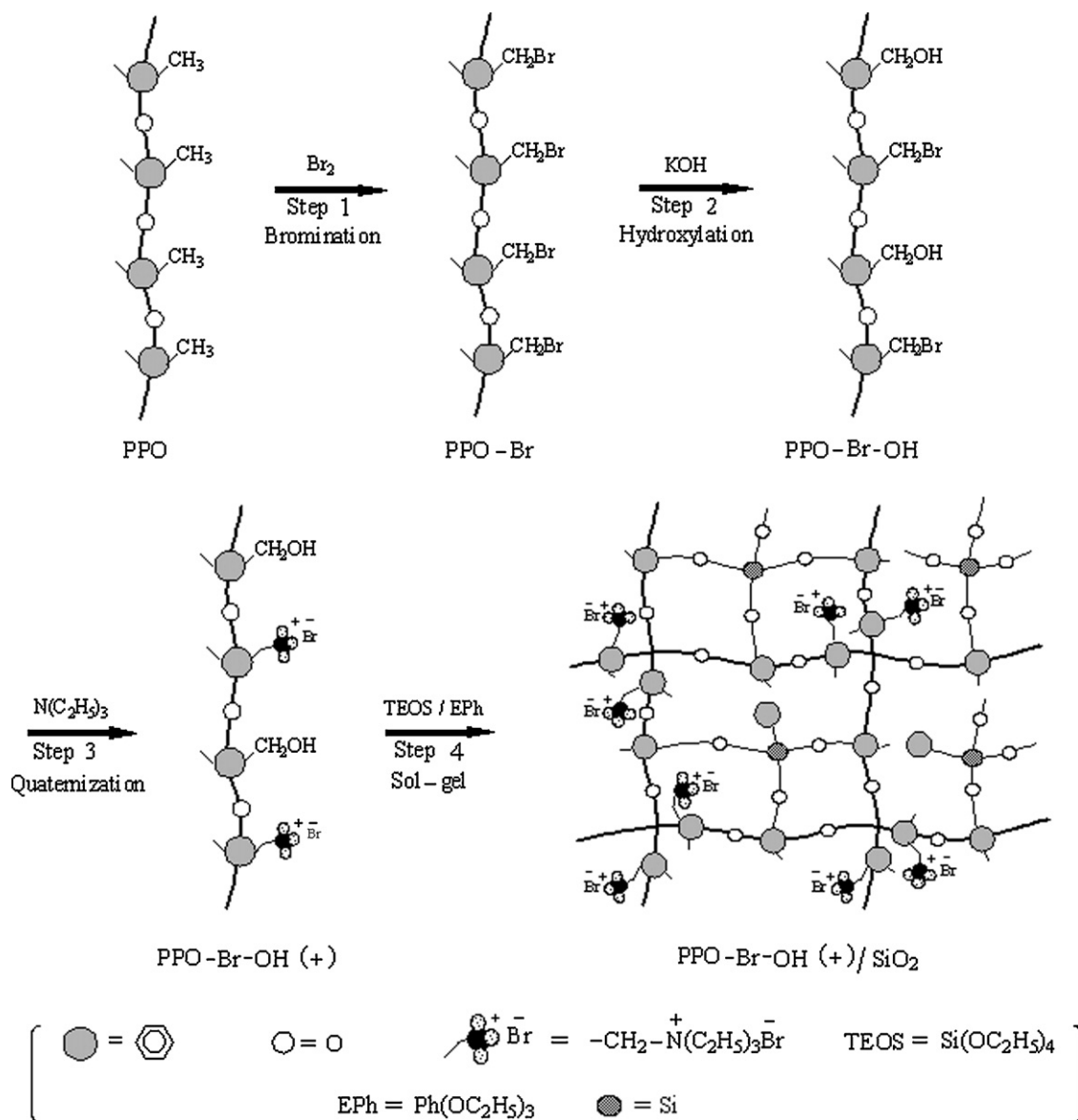
Scheme 1. The preparation of silica–polymer hybrid membranes based on poly(2,6-dimethyl-1,4-phenylene oxide) (PPO).

In this study, we extend on the previous hybrid membrane work and perform substantial modifications to the preparation procedures, including silica contents and increase in the cross-linking degree between PPO polymer and silica, to optimize the resultant properties of the membranes. The aim was to improve swelling resistance, while significantly enhancing the conductivity with no loss of thermal and chemical stability. The beginning-of-life single cell performance of an optimized membrane was also evaluated.

2. Materials and methods

2.1. Preparation of hybrid membranes

Poly(2,6-dimethyl-1,4-phenylene oxide) (PPO) of intrinsic viscosity $0.057\,dm^3\,g^{-1}$ in chloroform at $25\,°C$ (approximate molecular weight 90,000) was kindly supplied by the Institute of Chemical Engineering of Beijing (China). Chlorobenzene of analytical grade was stored over molecular sieve before use. Deionized water (grade II) was used throughout. All the other reagents were of analytical grade and used as received.

The preparation of PPO–silica hybrid membranes was in four steps: bromomethylation, partial hydrolysis, quaternization and a final sol–gel process (Scheme 1). The procedures have been described in detail previously [16] but are summarized here with the emphasis on the optimizations. Bromomethylation was performed by mixing bromine and PPO (molar ratio 1.5:1), both of which were diluted by chlorobenzene at $135\,°C$ for $10\,h$. The product was cut into pieces of film (approximately $60\,\mu m$ thick and $2\,cm \times 4\,cm$ wide) and was subsequently partially hydrolyzed by immersion of the films in aqueous KOH ($1\,mol\,dm^{-3}$) at $60\,°C$ for $24\,h$. Compared with our previous work [16], the reaction conditions were modified in anticipation of a higher degree of reaction, including an increase in reaction time for the bromomethylation (previously $8\,h$), increase of KOH concentration (previously $0.5\,mol\,dm^{-3}$) and increase of hydrolysis temperature (previously $55\,°C$). The partially hydrolyzed product was subsequently dissolved in chlorobenzene, followed by addition of DMF and triethylamine. This quaternization step was continued at $40\,°C$ for $13\,h$, during which ethanol was added at a controlled rate (about $1.4\,cm^3\,min^{-1}$) so that a homogeneous solution was maintained. The products from these first three

Table 1
Select properties of alkaline membranes A–G.

	Membrane						
	A	B	C	D	E	F	G
Theoretical silica content (%)	0	2.8	5.4	7.8	10.0	12.0	13.9
IDT (°C)[a]	176.1	186.3	198.3	187.4	185.5	186.9	186.0
T_d (°C)[b]	194.3	209.0	221.2	210.9	210.6	213.8	211.5
Thickness (μm)	151	129	140	126	120	123	133
Conductivity (S cm^{-1})	0.0079	0.0099	0.0110	0.0094	0.0097	0.0095	0.0080

[a] IDT is the initial decomposition temperature determined from the TG thermograms.
[b] The thermal degradation temperature (T_d) is defined as the temperature at which a weight loss = 5% occurs in the TG thermograms.

steps are denoted as PPO–Br, PPO–Br–OH, PPO–Br–OH(+), respectively.

The subsequent sol–gel reaction was performed by addition of monophenyltriethoxysilane (EPh), tetraethoxysilane (TEOS), and H$_2$O: the molar ratio of EPh to TEOS was fixed at 1:1. The molar percent of EPh with respect to benzyl groups of PPO polymer was varied from 0, 6.25, 12.5, 18.75, 25, 31.25 to 38%. This is different from the ratio previously reported (fixed at 12.5% [16]). After being stirred at 40 °C for 24 h, the solution was cast on a Teflon plate, dried in air at room temperature for 2 days, further heated to 130 °C (initially at the rate of 5 °C h^{-1} and then held at this temperature for 5 h) to get the final hybrid membranes. Note that the highest heating temperature was set to 130 °C since our previous work confirmed that this yields the optimum membrane properties. The seven membranes obtained are denoted as A–G accordingly (Table 1) with theoretical silica contents (SiO$_2$) of 0, 2.8, 5.4, 7.8, 10.0, 12.0, and 13.9%, respectively.

2.2. Membrane characterization

^{1}H NMR spectra of PPO, PPO–Br and PPO–Br–OH were recorded on a Bruker DMX-300 NMR instrument at 300 Hz with CDCl$_3$ used as solvent, and tetramethylsilane as internal standard. ^{29}Si NMR experiments were performed with an Infinity Plus-300 (Varian Inc., USA) instrument, and the samples were in the form of powder, prepared by grinding of the test film. FTIR spectra of the samples were recorded using FTIR spectrometer (Vector 22, Bruker) with a resolution of 2 cm^{-1} and a spectral range of 4000–400 cm^{-1}. The thermal behavior was analyzed with a Shimadzu TGA-50H analyzer under air flow and with a heating rate of 10 °C min^{-1}.

Ion-exchange capacities (IECs) were measured in the similar way to previous works [20]. Dry samples were accurately weighed and converted to the Cl$^-$ form in aqueous NaCl (1 mol dm^{-3}) for 2 days. Excessive NaCl was washed out and then the samples were immersed in aqueous Na$_2$SO$_4$ (0.5 mol dm^{-3}) for 2 days. Anion-exchange capacities were obtained by determining the amount of the exchanged Cl$^-$ through potentiometric titration with aqueous AgNO$_3$ (0.1 mol dm^{-3}).

Water uptakes (W_R) were measured as follows [20]: the samples were immersed in water at 25 °C for 2 days. Surfaces of the wet samples were then carefully dried prior to weighing. W_R was calculated as the relative weight gain on hydration per gram of the dry sample.

The morphologies of hybrid membranes were observed with a scanning electron microscopy (XT30 ESEM-TMP PHILIP). Before observation, surface or cross-sections of membranes were coated with gold.

The tensile properties were measured using an Instron universal tester (Model 1185) at room temperature, with dumbbell shape specimens at a crosshead speed of 25 mm min^{-1}, and with an initial gauge length of 25 mm. Tensile strength (TS) and elongation at break (E_b) values were recorded.

The membrane conductivity was measured using normal standard four-point probe technique [20]. Before measurement, the membranes were transformed to OH$^-$ form through immersing in aqueous KOH solution (0.5 mol dm^{-3} for 2.5 h and then 2 mol dm^{-3} for 4 h). Subsequently, they were washed free of the excess absorbed KOH, and kept in water throughout. Two samples (1 cm wide and 4 cm) for each membrane were used. One sample was for the measurement at room temperature, which took about 1–2 min. The other was kept in water vapor condition (in an electric cooker) for the measurement at elevated temperature, and it took less than 1 h to fulfill the whole measurement from 30 °C to 90 °C. All these actions were taken to ensure that the membrane samples had less chance to contact air and hence keep mainly in OH$^-$ state during the measurement. The Teflon measuring cell contained two stainless steel flat outer current-carrying electrodes (2 cm apart) and two platinum wire inner potential-sensing electrodes (1 cm apart). Membrane samples were mounted into the cell and the screws were tightened to a constant torque to ensure good membrane–electrode contact and reproducible results. The impedance was determined using an Autolab PGSTAT 30 (Eco Chemie, Netherland, with FRA2 module) under galvanostatic mode with ac perturbation current amplitude of 0.1 mA over the frequency range from 1 MHz to 50 Hz. A Bode plot was plotted to check the frequency region where the impedance had a constant value, and the resistance was obtained from the associated Nyquist plot. The hydroxyl ion (OH$^-$) conductivity (σ) was calculated according to:

$$\sigma = \frac{L}{RWd}$$

where R is the obtained membrane resistance, L the distance between potential-sensing electrodes, W and d the wide and thickness of the membrane sample, respectively.

Fuel cell testing was conducted according to previous reports [3,21]. The anode and cathode electrodes were both commercial (E-Tek) type with Pt/C (20% mass) catalyst on one side at a loading of 0.5 mg cm^{-2} Pt loading bound (PTFE binder) to a carbon microporous layer on top of a Toray carbon paper (TGPH-090) backing layer. The electrodes are treated with SION1 (Surrey Ionomer Concept 1): a solution of poly(vinylbenzyl chloride) dissolved in ethyl acetate was sprayed onto the catalyzed side of each electrode to 0.5 mg$_{polymer}$ cm^{-2} loading and then they were immersed in N,N,N',N'-tetramethylhexane-1,6-diamine. After washing with water, the electrodes were converted to OH$^-$ form by soaking in aqueous KOH (1 mol dm^{-3}) and assembled into a single fuel cell along with membrane C with no pre-pressing. The electrode areas were 25 cm^2. Fuel cell testing was conducted at 50 °C, with H$_2$ and O$_2$ gases flowing at 2 dm^3 min^{-1} rate and controlled at 100% relative humidity. No back pressurization was used.
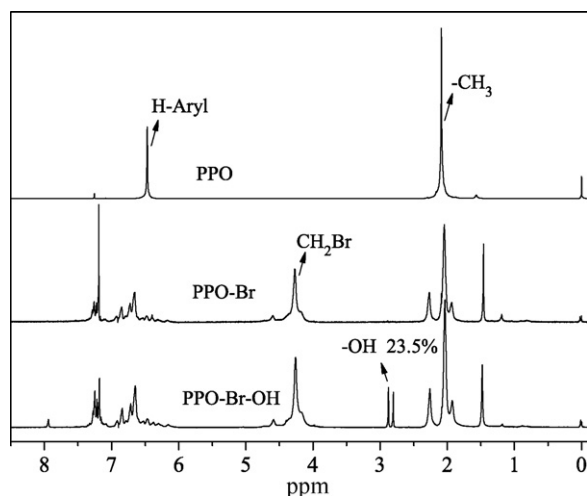
Fig. 1. ^{1}H NMR spectra of PPO, PPO–Br and PPO–Br–OH membranes.

3. Results and discussion

3.1. ^{1}H NMR spectra of PPO, PPO–Br and PPO–Br–OH

The ^{1}H NMR spectra for each stage of the synthesis are shown in Fig. 1, where the characteristic proton resonance signals are identified in-line with previous studies [16]. In the spectrum of PPO–Br, there is a strong peak at δ = 4.4 not observed for the starting PPO, indicating the existence of –CH$_2$Br [16]. The benzyl substitution ratio in PPO–Br, as calculated from the relative magnitude of integrating peak intensities for –CH$_2$Br and phenyl groups, is 95%. New peaks at δ = 2.80–2.87 appear in the spectra of PPO–Br–OH, indicating the existence of benzyl-OH groups. From the relative magnitude of benzyl-OH and phenyl integrating peak intensity, the degree of hydroxylation is calculated as 23%.

The benzyl substitution ratio and hydroxylation degree are higher than those reported previously (87 and 2.8%, respectively [16]). Higher hydroxyl group (–OH) content in the polymer chains will lead to enhanced cross-linking between the organic PPO polymer chains and the silica, as they partially take part in the sol–gel process to form Si–O–C covalent linkages (Scheme 1).

3.2. FTIR spectra of membranes A–G

FTIR spectra of membranes A–G are shown in Fig. 2. All the spectra show a large band between 3100 cm^{-1} and 3700 cm^{-1}, which
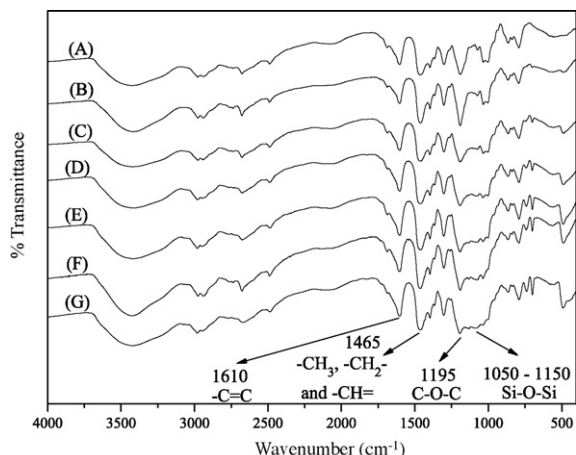

Fig. 2. The FTIR spectra of membranes A–G.

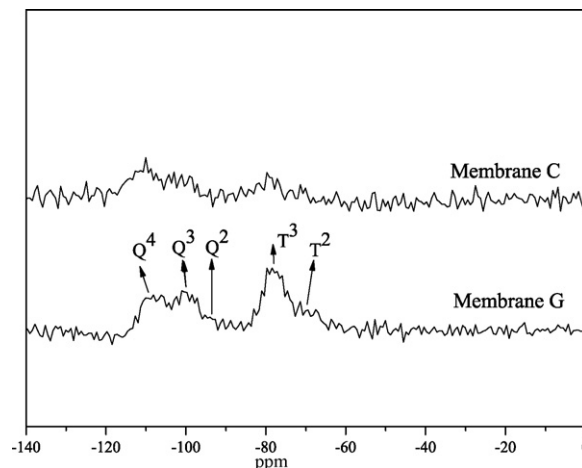**Fig. 3.** Solid-state ^{29}Si NMR spectra of membranes C and G.

is ascribed to the stretching vibration of –OH groups from Si–OH groups and absorbed water. The bands in the 2850–3050 cm^{-1} region and at 1465 cm^{-1} are from the stretching of CH$_3$–, –CH$_2$– and =CH– groups (ν and δ). The band at 1610 cm^{-1} is attributed to the C=C stretching vibration in phenyl groups ($\nu_{C=C}$); the peaks at 1195 cm^{-1} are characteristic of C(=O)–O–C stretching, and 1050–1150 cm^{-1} are characteristic of –Si–O–Si– stretching [7].

The intensity of –Si–O–Si– (1050–1150 cm^{-1}) bands increases in accordance with the increasing silica content from membrane A to membrane G as expected. However, the intensities of CH$_3$–, –CH$_2$– and =CH– (1465 cm^{-1}) bands are similar, indicating these membranes have equivalent contents of quaternary ammonium groups.

3.3. ^{29}Si NMR and morphology of membranes A–G

Solid-state ^{29}Si NMR spectra of membranes C and G are presented in Fig. 3. The region ranging from δ = −113 to −93 is credited to the siloxanes arising from the TEOS precursor and includes the three peaks at δ = −95, −100, and −109 arising from di-, tri- and tetra-substituted silicates [22] (Q^2, Q^3 and Q^4). The region from δ = −67 to −83 is due to the silicates from the EPh precursor and includes peaks arising from di- and tri-substituted silicates (T^2 and T^3) at δ = −78 and −71 [23]. The intensities of the Q^4, Q^3 and T^3 signals are higher than those for the Q^2 and T^2 silicates, which indicate a high degree of siloxane condensation in the hybrid membranes. Membrane G has the higher silica content and shows more intense and visible signals compared to membrane C.

The morphologies of membranes A and E, as observed using SEM, are presented in Fig. 4, and are visibly compact, smooth, and homogenous. Hence, membranes containing up to 10% silica content retain integrity and homogeneity. The homogeneity is attributed to the favorable interaction between the organic PPO and inorganic silica phases via both covalent bonds and weak bonds (such as van der Waals, hydrogen and ionic interactions [16]). Membrane F is less homogenous with visible particles (less than 0.5 μm in size) due to some congregation of the Si–O–Si network. Membrane G is rough and contains larger silica particles (up to 1 μm), indicating that this membrane has a significant level of undesirable phase separation.

3.4. Short-term thermal stabilities

TGA was used to determine the short-term thermal stabilities of membranes A–G, and the thermograms are presented in Fig. 5. Since the membranes were treated at 130 °C for 5 h, the
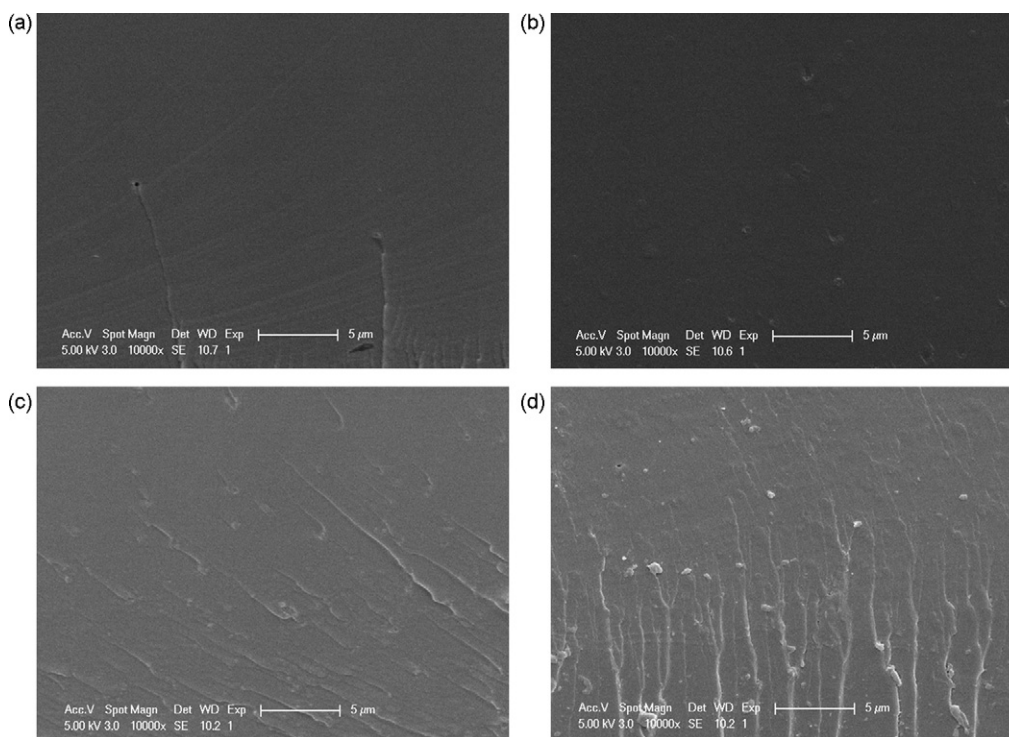
Fig. 4. SEM micrographs of (a) membrane A, (b) membrane E, (c) membrane F, and (d) membrane G.

weight losses below 130 °C were attributed to the evaporation of absorbed water. The initial decomposition temperatures (IDT) and thermal degradation temperatures (T_d: defined as the temperature at 5% weight loss that was not due to water loss) are summarized in Table 1. The IDT values are all above 176 °C, and the T_d values are in the narrow range 194–221 °C. Although these values are slightly lower than for fluoropolymer-based membranes (IDT up to 194 °C) [24], they are similar to a number of other reported non-fluoropolymer-based alkaline membranes that have been developed for fuel cell applications [25–27].

Compared with membrane A, membranes B–G have higher IDT values, indicating of the potentially greater stability of the hybrid membranes relative to the corresponding inorganic-free organic control membrane. Membrane C had the highest IDT value indicated that a silica content of 5.4% is optimal [7]. Generally, as the silica content increases, the thermal stability should increase due to increasing levels of cross-linking. However, we have already seen

that if the silica content is too high, the membrane's homogeneity may be compromised.

3.5. Ion-exchange capacity (IEC) and water uptake (W_R)

The IECs of membranes A–G, presented in Fig. 6, are in the range of 2.0–2.3 mmol g^{-1}, which are higher when compared to previous membranes of this type (0.76–2.12 mmol g^{-1}) [16]. This is attributed to the increase in PPO–Br benzyl substitution ratio (95%). The higher IECs are expected to enhance membrane conductivity. From membrane B to membrane G, the IECs decrease from 2.3 mmol g^{-1} to 2.0 mmol g^{-1} due to the dilution effect of the uncharged silica component. However, the silicate-free membrane A has an abnormally low IEC value (2.1 mmol g^{-1}). This results from the increased degradation of quaternary ammonium groups ($-N(C_2H_5)_3{}^+$) of membrane A during the long time-frame thermal treatment [16] as membrane A exhibited the lowest IDT value.
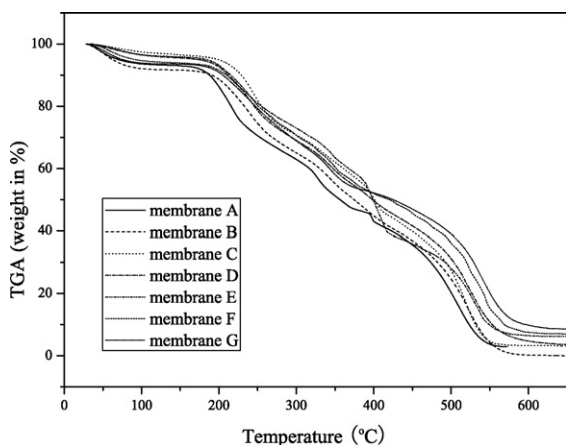

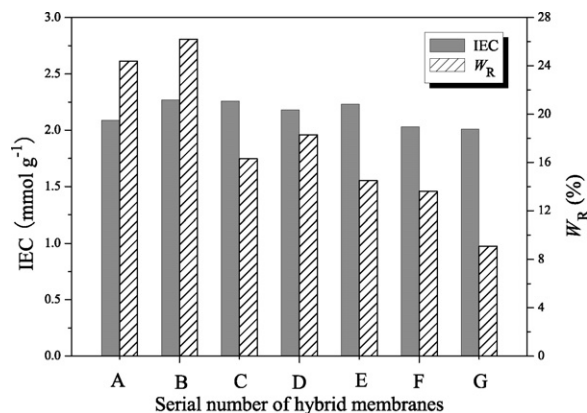**Fig. 5.** TG thermograms of membranes A–G under air flow with a heating rate of 10 °C min^{-1}.

Fig. 6. The water uptakes (W_R) and ion-exchange capacities (IEC) of membranes A–G.
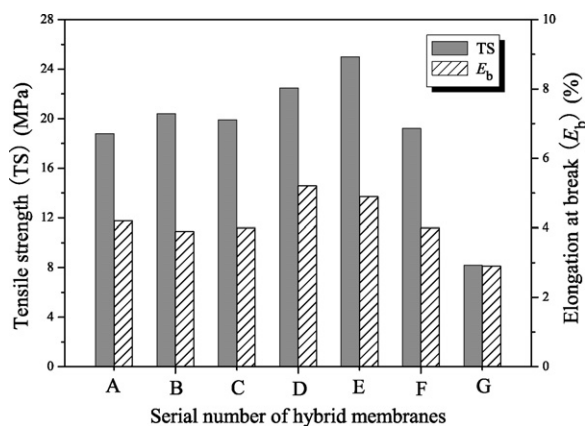
Fig. 7. The tensile strength (TS) and elongation at break (E_b) values of membranes A–G.

Fig. 8. The ionic conductivity of membranes B–D compared to a selection of previously reported membranes, including FEP-based membranes [30], PVA/TiO$_2$ hybrid membranes [32], and PVA-based organic membranes [11].

Water uptake (W_R) are also presented in Fig. 6 and ranged from 9.1 to 26%. The values are distributed in a narrower range and at a generally lower level when compared with our previous membranes (2.0–179 [16]). The lower uptakes are desirable for lowering membrane swelling and for retention of dimensional stability when the membranes are exchanged from the Br$^-$ form to the OH$^-$ form. To confirm this point, the W_R values of the membranes in the OH$^-$ form were also measured; the values were in the range 32–64%, which are much lower than those of previous membranes (34 to more than 1000% [16]).

3.6. Tensile properties

The tensile strengths (TS; Fig. 7) are in the range 8.2–25.0 MPa, and the elongations at break (E_b) are 2.9–5.2%. Compared with previously reported nylon fiber membranes (TS = 4.6–10.1 MPa and E_b = 16.7–42.6% [28]) and rubbery epoxy mesocomposites (TS < 5.5 MPa, and E_b = 20–35% [29]), our membranes have promising tensile properties with higher levels of TS but lower E_b values. An increase in silica content induces an initial increase in TS from 18.8 MPa (membrane A) to 25.0 MPa (membrane E) and then a decrease to 8.2 MPa (membrane G). This indicates that an optimal silica content enhances strength but excessive silica contents, which destroys homogeneity, reduces membrane strength. Optimal silica content is also desirable for preparing flexible membranes, and as such membranes D had the highest E_b of 5.2%.

3.7. Membrane conductivity

At room temperature and under fully hydrated conditions, the OH$^-$ conductivity of membranes thickness in the range of 120–151 μm, were in the range 0.008–0.011 S cm^{-1} (Table 1). The OH$^-$ conductivity values are approaching those of fluoropolymer-based membranes (0.01–0.016 S cm^{-1} at room temperature [30]), and slightly higher than those of our previous membranes (0.001–0.009 S cm^{-1} [16]) and for other reported membrane types, such as 4-vinylpyridine-based membranes (0.0005–0.0043 S cm^{-1} [31]) and cross-linked PVA/TiO$_2$ composite membrane (0.0056 S cm^{-1} [32]). Hybrid membranes B–G have higher conductivity values than membrane A, indicating certain levels of silica content can enhance ionic conductivity. Membrane C, with 5.4% silica, has the highest room temperature conductivity.

Membrane ionic conductivity is affected by the ion concentration and mobility, hydration levels, and polymer structure/chain mobility [33]. To date, the influence of inorganic silica component on membrane conductivity has been extensively investigated and debated but there is still n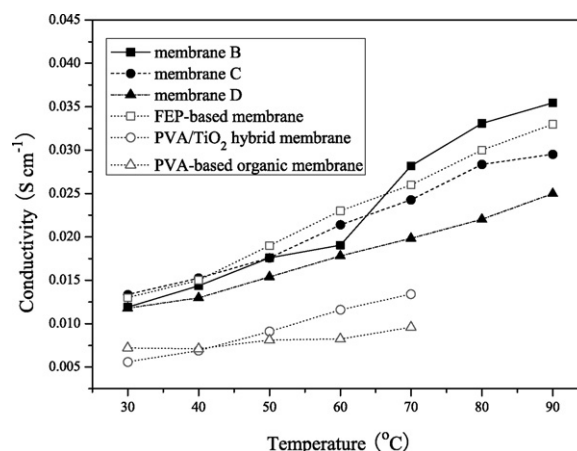o agreement. On one hand, cross-linked Si–O–Si network may limit the mobility of the conductive ions and hinder the formation of conductive and hydrophilic ionic clusters and channels (as found with the perfluorosulfonic acid polymer electrolytes). Therefore, a decrease in ion conductivity on incorporation of silica is often reported [34,35]. On the other hand, hydroxyl groups (–SiOH) from silica have strong bonding ability with H$_2$O molecules and are thus favorable for water retention and therefore ion transfer [36]. Therefore, there is a mechanism where addition of silica can enhance ion conductivities [36]. Our present, and previous work on hybrid membranes based on poly(styrene-co-methylmethacrylate)–silica [7], both support the latter.

As has been reported, operation of AMFCs at elevated temperatures [3] lead to enhanced performances. High temperatures would not only reduce thermodynamic voltage losses due to potential pH gradients through the membrane but also improve electrokinetics [1]. For feasibility testing of potential use in fuel cells the conductivities of membranes B–D, with higher short-term thermal stabilities, were measured over a range of elevated temperatures (Fig. 8). It is important to note that our prior hybrid membranes were not suitable for the measurement at temperatures above 60 °C due to their high swelling degrees [16]. The performances of a selection of membranes from other groups, including FEP-based membranes [30], PVA/TiO$_2$ hybrid membranes [32], and PVA-based organic membranes [11], were used for comparison. From 30 °C to 90 °C, the conductivities of membranes B–D increased from 0.012 S cm^{-1} to 0.035 S cm^{-1}. These values are comparable to those of FEP-based membranes, and much higher than those of PVA/TiO$_2$ hybrid membranes and PVA-based organic membranes (0.006–0.013 S cm^{-1}). Membrane C has higher conductivities than membrane D at all temperatures and higher values than membrane B below 60 °C. From membrane B to membrane D, the changing tendency of conductivity becomes more linear. Hence, membrane C (5.4% silica) was selected for evaluation in AMFCs.

The dependence of ionic conductivity on temperature for low temperature polymer electrolytes is typically taken as Arrhenius type:

$$\sigma = \sigma_0 \exp \left(-\frac{E_a}{RT} \right)$$

where σ_0 is a pre-exponential factor, E_a is the activation energy, and T is the thermodynamic temperature in K. The activation energy (E_a) of membranes can be obtained from plots of $\ln(\sigma)$ versus $1/T$ (see Fig. 9). From membrane B to membrane D (increasing silica contents), Ea values decrease from 18 kJ mol^{-1} to 12 kJ mol^{-1}. These values are comparable to those of previously reported alka-

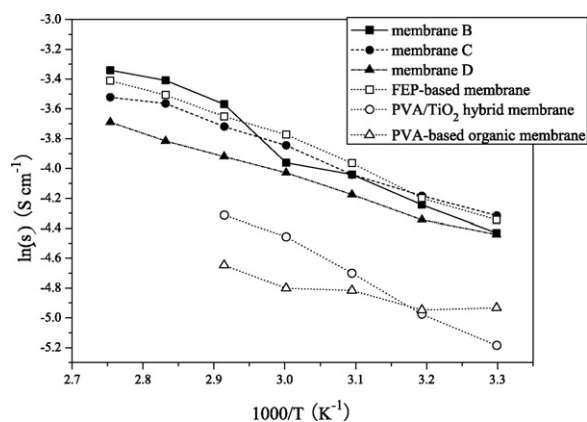**Fig. 9.** The Arrhenius plots obtained from the data in Fig. 8.

line membranes (14.8 kJ mol^{-1} for FEP-based membranes [30], 19.6 kJ mol^{-1} for PVA/TiO$_2$ hybrid membranes [32] and 6.2 kJ mol^{-1} for PVA-based organic membranes [11]).

3.8. Fuel cell performances

Membrane C (5.4% silica, thickness = 140 μm, W_R = 30.9%, σ = 0.011 S cm^{-1} at room temperature and σ = 0.018 S cm^{-1} at 50 °C) was used for an initial fuel cell performance evaluation. The single cell employing the membrane was operated at 50 °C (β-hydrogen-containing SION1 limits the fuel cell tests to <55 °C) and fed with high purity and fully humidified hydrogen and oxygen gases at the anode and cathode, respectively. After a 2 h activation at a high current cell discharge at 0.05 V (required for SION1), the performance of the cell was recorded (Fig. 10).

The cell exhibited an open circuit voltage (OCV) of 1.04 V, which is similar to cells using radiation-grafted membranes [21]. The peak power density of the cell was 32 mW cm^{-2} at a current density of 80 mA cm^{-2}. The value is comparable to those recorded for non-fluorinated quaternary ammonium membranes (20–42 mW cm^{-2} [37]), but lower than those of radiation-grafted membranes, such as 56 mW cm^{-2} for thick membranes (153 ± 4 μm when fully hydrated and 133 ± 4 μm when fully dehydrated [21]), and 230 mW cm^{-2} for thin membranes (18 μm when fully hydrated and 15 μm when fully dehydrated [10]). The relatively lower peak power density is partially due to the high thickness of membrane C (140 μm), since high thickness is disadvantageous to the power performance of alkaline membrane fuel cells under these test conditions [3,38]. Higher peak power densities are anticipated with the use of thinner membrane samples (lower than 50 μm) and optimized electrodes (coated in ionomers that have better chemical
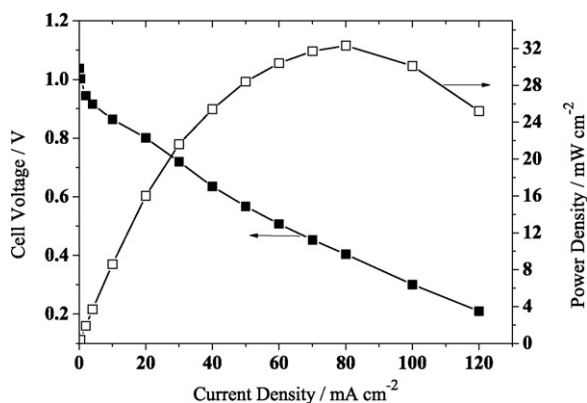
compatibility to the membranes). Lower membrane thickness can be achieved with adjustment of the concentration and viscosity of the sol–gel casting solution, and the choice of suitable casting plate.

After a long-term fuel cell testing, the membrane has a little dissolution, indicating that the stability under testing conditions needs to be further improved. Besides, the ionomer used in this work cannot endure high temperature due to the existence of β-hydrogen. In our following work, further modifications are to be utilized to improve the long-term stability of the hybrid membranes, including the change of the bromination degree of PPO–Br, replacement of triethylamine with trimethylamine as the quaternization agent. In this way, the relatively unstable β-hydrogen can be avoided and the thermal stability enhanced, which has been confirmed by our recent work of PPO-based diffusion dialysis membranes [39]. The PPO-based hybrid material may also be tried as the ionomer. Its adhesion to the hybrid membranes would be more excellent. The related work is underway and will be reported in due course.

4. Conclusion

Organic–inorganic hybrid anion-exchange membranes were prepared by incorporation of silica into poly(2,6-dimethyl-1,4-phenylene oxide)(PPO). Compared with previous PPO–silica hybrid membranes [16], these membranes exhibited improved swelling resistance and high ion-exchange capacities (2.01–2.27 mmol g^{-1}) with initial indications of good thermal and mechanical stabilities. Hydroxide anion conductivities of up to 0.011 S cm^{-1} were obtained at room temperature and up to 0.035 S cm^{-1} at 90 °C. These results indicate a successful optimization of the chemical composition of the PPO-based hybrid membranes.

Membranes with 2.8–7.8% silica content show the best performances with short-term thermal stabilities higher than 186 °C, tensile strengths in the range of 20–23 MPa, elongation at break values up to 5.2%, IECs in the range of 2.2–2.3 mmol g^{-1}, and good swelling resistances. A thick 140 μm membrane with 5.4% silica was tested in a single cell fuel cell and a peak power density of 32 mW cm^{-2} was obtained. Hence, these hybrid membranes show promise for application in alkaline membrane fuel cells (AMFCs) and further research is on-going to reduce the thickness and develop a chemically compatible ionomer.

Fig. 10. The H$_2$/O$_2$ fuel cell performances of membrane C at 50 °C.

References

[1] J.R. Varcoe, R.C.T. Slade, Fuel Cells 5 (2005) 187–200.
[2] S. Lu, J. Pan, A. Huang, L. Zhuang, J. Li, Proc. Natl. Acad. Sci. U.S.A. 105 (2008) 20611–20614.
[3] J.R. Varcoe, R.C.T. Slade, Electrochem. Commun. 8 (2006) 839–843.
[4] E.H. Yu, K. Scott, J. Power Sources 137 (2004) 248–256.
[5] J.R. Varcoe, R.C.T. Slade, E.L.H. Yee, S.D. Poynton, D.J. Driscoll, D.C. Apperley, Chem. Mater. 19 (2007) 2686–2693.
[6] K. Matsuoka, Y. Iriyama, T. Abe, M. Matsuoka, Z. Ogumi, J. Power Sources 150 (2005) 27–31.
[7] Y.H. Wu, C.M. Wu, T.W. Xu, F. Yu, Y.X. Fu, J. Membr. Sci. 321 (2008) 299–308.
[8] D. Stoica, L. Ogier, L. Akrour, F. Alloin, J.-F. Fauvarque, Anionic membrane based on polyepichlorhydrin matrix for alkaline fuel cell: synthesis, physical and electrochemical properties, Electrochim. Acta 53 (2007) 1596–1603.
[9] H. Herman, R.C.T. Slade, J.R. Varcoe, J. Membr. Sci. 218 (2003) 147–163.
[10] J.R. Varcoe, M. Beillard, D.M. Halepoto, J.P. Kizewski, S.D. Poynton, R.C.T. Slade, Electrochem. Soc. Trans. 16 (2008) 1819–1834.
[11] Y. Xiong, J. Fang, Q.H. Zeng, Q.L. Liu, J. Membr. Sci. 311 (2008) 319–325.
[12] L. Li, Y.X. Wang, J. Membr. Sci. 262 (2005) 1–4.
[13] J. Fang, P.K. Shen, J. Membr. Sci. 285 (2006) 317–322.

[14] S. Gu, R. Cai, T. Luo, Z. Chen, M. Sun, Y. Liu, G. He, Y. Yu, Angew. Chem. Int. Ed. 48 (2009) 6499–650211.
[15] L. Wu, T.W. Xu, D. Wu, X. Zheng, J. Membr. Sci. 310 (2008) 577–585.
[16] Y.H. Wu, C.M. Wu, T.W. Xu, X.C. Lin, Y.X. Fu, J. Membr. Sci. 338 (2009) 51–60.
[17] T.W. Xu, D. Wu, L. Wu, Prog. Polym. Sci. 33 (2008) 894–915.
[18] Y. Xiong, Q.L. Liu, A.M. Zhu, S.M. Huang, Q.H. Zeng, J. Power Sources 186 (2009) 328–333.
[19] T.N. Danks, R.C.T. Slade, J.R. Varcoe, J. Mater. Chem. 12 (2002) 3371–3373.
[20] Y.H. Wu, C.M. Wu, F. Yu, T.W. Xu, Y.X. Fu, J. Membr. Sci. 307 (2008) 28–36.
[21] J.R. Varcoe, R.C.T. Slade, E.L.H. Yee, Chem. Commun. (2006) 1428–1429.
[22] D.S. Kim, H.B. Park, Y.M. Lee, Y.H. Park, J.W. Rhim, J. Appl. Polym. Sci. 93 (2004) 209–218.
[23] H.Y. Chang, R. Thangamuthu, C.W. Lin, J. Membr. Sci. 228 (2004) 217–226.
[24] T.N. Danks, R.C.T. Slade, J.R. Varcoe, J. Mater. Chem. 13 (2003) 712–721.
[25] I. Honma, S. Nomura, H. Nakajima, J Membr. Sci. 185 (2001) 83–94.
[26] M. Popall, X.M. Du, Electrochim. Acta 40 (1995) 2305–2308.
[27] S.Y. Lee, G. Scharfenberger, W.H. Meyer, G. Wegner, J. Power Sources 163 (2006) 27–33.
[28] Y. Li, Z.M. Huang, Y.D. Lv, Eur. Polym. J. 42 (2006) 1696–1704.
[29] I. Park, H.G. Peng, D.W. Gidley, S. Xue, T.J. Pinnavaia, Chem. Mater. 18 (2006) 650–656.
[30] R.C.T. Slade, J.R. Varcoe, Solid State Ionics 176 (2005) 585–597.
[31] K. Matsuoka, S. Chiba, Y. Iriyama, T. Abe, M. Matsuoka, K. Kikuchi, Z. Ogumi, Thin Solid Films 516 (2008) 3309–3313.
[32] C.C. Yang, J. Membr. Sci. 288 (2007) 51–60.
[33] K.D. Kreuer, S.J. Paddison, E. Spohr, M. Schuster, Chem. Rev. 104 (2004) 4637–4678.
[34] R.Q. Fu, J.J. Woo, S.J. Seo, J.S. Lee, S.H. Moon, J. Power Sources 179 (2008) 458–466.
[35] M. Kato, W. Sakamoto, T. Yogo, J. Membr. Sci. 311 (2008) 182–191.
[36] Y.M. Kim, S.H. Choi, H.C. Lee, M.Z. Hong, K. Kim, H.I. Lee, Electrochim. Acta 49 (2004) 4787–4796.
[37] E. Agel, J. Bouet, J.F. Fauvarque, J. Power Sources 101 (2001) 267–274.
[38] J.R. Varcoe, R.C.T. Slade, G.L. Wright, Y. Chen, J. Phys. Chem. B 110 (2006) 21041–21049.
[39] J.Y. Luo, C.M. Wu, Y.H. Wu, T.W. Xu, J. Membr. Sci. 347 (2010) 240–249.